Solubility of Gaseous Carbon Dioxide in Molten LiCl-Li_2O

Takafumi Wakamatsu*[a], Takuya Uchiyama[a], Shungo Natsui[a], Tatsuya Kikuchi[a], Ryosuke O. Suzuki**[a]

[a] Division of Materials Science and Engineering, Faculty of Engineering, Hokkaido University, Kita-13Jou, Nishi-8 Chome, Kita-ku, Sapporo, Hokkaido 060-8628, Japan

*First author: +81-11-706-6341,t.wakamatsu@eng.hokudai.ac.jp

**Corresponding author: +81-11-706-6339, rsuzuki@eng.hokudai.ac.jp

Abstract

Carbonate ions in LiCl-Li_2O salt are a source of carbon contamination in the electrolytic refining of metal oxides, and their concentration is also essential information for understanding the CO_2 decomposition process. In this study, the solubility of gaseous CO_2 in molten LiCl-Li_2O was studied, with the goal of developing processes to decompose the oxides effectively. Ar-CO_2 gas mixtures were dissolved in molten salts containing various amounts of Li_2O, and the solubility of the CO_2 gas was calculated by measuring the mass difference between the molten salts before and after the CO_2 dissolution. The molar amount of dissolved CO_2 gas was almost as large as the molar

quantity of Li_2O when the partial pressure of CO_2 was 1.0 or 0.5 atm for Li_2O concentrations in the range of 0–60 mol%. This confirms that a large quantity of the oxide ions reacted with the CO_2 gas, resulting in the generation of carbonate ions.

Keywords: molten salt; solubility; phase diagram; carbon dioxide

1. Introduction

Several methods for the electrochemical reduction of metal oxides using molten salts have been actively developed in the past decades [1-9]. For example, the OS (Ono-Suzuki) process and the FFC (Fray-Farthing-Chen) process have become well known methods for reducing titanium oxide in $CaO\text{-}CaCl_2$ [2,4]. In the OS process, the metallic calcium electrodeposited on the cathode dissolves into the molten salt to create an environment that can reduce metallic oxides such as TiO_2. Subsequently, calcium oxide is formed as a product of a calciothermic reaction and is electrolyzed in the molten salt. At the anode, carbon reacts with oxide ions and forms carbon dioxide or carbon monoxide, which removes oxygen from the molten salt [2]. On the other hand, the FFC process is a direct reaction in which a metallic oxide is used as the cathode, where it is reduced electrochemically to remove oxygen ions [4].

The electrochemical and thermochemical reactions involved in these mechanisms can

be summarized as follows:

OS process

$Ca^{2+} + 2e^- \rightarrow Ca$ (at the cathode) (1)

$Ca \rightarrow \underline{Ca}$ (dissolution to molten salt) (2)

$n\underline{Ca} + M_mO_n \rightarrow mM + nCaO$ (reduction) (3)

$CaO \rightarrow Ca^{2+} + O^{2-}$ (ionization) (4)

$nO^{2-} + C \rightarrow CO_n + 2ne^-$ (n = 1 or 2) (at the anode) (5)

FFC - Cambridge process

$M_mO_n + 2ne^- \rightarrow mM + nO^{2-}$ (electroreduction at the cathode) (6)

$nO^{2-} + C \rightarrow CO_n + 2ne^-$ (n = 1 or 2) (at the anode) (7)

In both processes, the dissolution of O^{2-} in the chloride melt is critically important to reduce the metallic oxide M_mO_n, and a high solubility of metallic Ca in the melt is also critical to realize good reactivity. The two molten salts, $CaCl_2$-CaO and LiCl-Li_2O, can reduce metallic oxides more efficiently than other combinations of oxides and chlorides.

The key advantage of both methods is that they enable the direct reduction of the

oxides. This is not true for the Kroll process conventionally used in industry, and thus these methods have the potential to replace it. However, the product is occasionally contaminated with carbon when the $CaCl_2$-CaO system is used [10], because the CO_2 gas evolved at the carbon anode partially dissolves into the salt as CO_3^{2-} and is reduced to carbon at the cathode. The resulting carbon deposits may react with the metallic particles, and produce a carbon solid solution or a carbide. Thus, it is very important to quantify the solubility of CO_2 in the molten salt in order to develop techniques to suppress the carbide formation and the carbonate reduction.

The CO_2 solubility in molten salts has been previously studied in order to understand the slag basicity in non-SiO_2-based fluxes [11-13]. Hashizume et al. [10] studied the solubility of CO_2 in the $CaCl_2$-CaO-$CaCO_3$ system from the viewpoint of phase equilibria and concluded that carbon contamination of the reduction product is caused by the following reaction (8):

$$CO_3^{2-} + 2Ca \rightarrow C + 3O^{2-} + 2Ca^{2+} \quad (8)$$

Oxide reduction in a LiCl-Li_2O melt is also popular, because it works even at low temperatures, but the CO_2 solubility and the concentration of CO_3^{2-} in this system have not been well examined. Therefore, the possibility of the occurrence of the following reaction (9) is considered in this study:

$$CO_3^{2-} + 4Li \rightarrow C + 3O^{2-} + 4Li^{+} \quad (9)$$

Otake et al. reported that CO_2 gas decomposes to carbon and oxygen in $CaCl_2$-CaO and LiCl-Li_2O melts [14]. The decomposition of the carbonate ions in the molten salt has also been examined and was found to be one of the reasons for the reduction of carbon from CO_2 gas [14, 15]. However, the dependence of the CO_3^{2-} concentration in molten LiCl-Li_2O on the melt composition, which is a fundamental property necessary for minimizing the contamination of the reduced product, has not been investigated in detail. In particular, melts in the LiCl-Li_2O system can decompose CO_2 at lower temperatures than those in the $CaCl_2$-CaO system, and a detailed study on CO_2 gas solutions in LiCl-Li_2O is desired both to analyze the decomposition process of CO_2 gas and to minimize the carbon contamination in the fresh product from the metallic oxide. Therefore, the present study aims to determine the solubility of CO_2 in molten LiCl-Li_2O and analyze the mechanism of CO_2 decomposition.

A temperature of 923 K was chosen for this study because evaporation is more significant above this temperature. Reliable and reproducible data have been obtained previously at 923 K, well above the melting temperature [25]. For example, Usami et al. [17] reported that 12 mol%Li_2O can dissolve in the LiCl melt at 923 K. Sanster et al. [16] measured the phase diagram of the LiCl-Li_2CO_3 system and found that the liquid

can exist at 923 K in a composition ranging between pure LiCl and 70 mol%Li_2CO_3. Assuming that the entire amount of Li_2O reacts with CO_2 to form Li_2CO_3, the solubility of Li_2CO_3 in LiCl is limited to 70 mol% at 923 K. Therefore, LiCl-Li_2O melts with various concentrations of Li_2O from pure LiCl to LiCl-70 mol%Li_2O were studied in this work.

2. Materials and methods

LiCl (99.0% purity, Wako Chemical Co.) and Li_2O (99.5% purity, Strem Chemicals Co.) were mixed to obtain the desired composition in the range of 0–60 mol% Li_2O and placed in an Al_2O_3 crucible with an inner diameter of 17 mm and height of 100 mm. The mass of the crucible after the mixture of salt and oxide was added was measured precisely before it was set inside the furnace. The crucible was fixed to a titanium rod and set inside the furnace, as shown in Fig. 1. The temperature of the furnace was controlled with an accuracy of ±1 K. The sample was dehydrated by continuous evacuation at 723 K. Then, the furnace was heated up to 923 K and filled with Ar gas. While this temperature was maintained, a gaseous Ar-CO_2 mixture was flowed through the furnace to dissolve into the molten salt for a predetermined time. The partial pressures of Ar and CO_2 gas in the mixture could be controlled in a range of

±0.004 atm. The crucible was retracted after the CO_2 flow was halted, and the crucible was cooled rapidly at the low-temperature zone in the upper part of the furnace. After the crucible cooled to room temperature, the mass of the crucible with the solidified salt was measured. The products in the crucible were characterized by powder X-ray diffraction (XRD) using CuKα radiation. The data processing procedures in this work are based on the general design of the experiments [24].

3. Results

Table 1 shows the experimental conditions and the results obtained.

3.1. Characterization of the products

Two samples with identical initial compositions of 30 mol% Li_2O were cooled and analyzed by XRD. To investigate the formation of carbonate in the presence of gaseous CO_2, two samples labeled #A and #B were prepared. Sample #A was heated without CO_2 even after the temperature reached 923 K. For sample #B, CO_2 was dissolved after the temperature was stabilized at 923 K. Fig. 2 shows the XRD patterns of these samples. Lithium oxide, lithium chloride, and lithium chloride hydrate were present in sample #A, as shown in Fig. 2(a). The hydrate was formed at room temperature because the lithium chloride easily reacts with moisture in the atmosphere during sample

handling for the XRD experiments. Although the intensities of the diffraction peaks of the hydrate increased when the sample was exposed to the atmosphere for a longer period, the initial constituents of sample #A, i.e., LiCl and Li_2O, did not change after the experiments, except for the formation of the LiCl hydrate. However, Li_2CO_3 was clearly generated because of the dissolution of CO_2 in sample #B, as shown in Fig. 2(b). Interestingly, peaks corresponding to lithium oxide disappeared in the XRD patterns of sample #B. The alumina peaks originated from the broken crucible.

Since the molten salt used in this study did not include network-forming entities such as SiO_2, lithium chloride and lithium oxide were completely ionized. Li_2CO_3 consists of lithium and carbonate ions, so the following reaction (10) takes place when CO_2 gas dissolves into the molten salt during heating [18-21]:

$$CO_2 + O^{2-} \rightarrow CO_3^{2-} \quad (10)$$

3.2. CO_2 saturation time

Even when a sufficient amount of CO_2 gas was introduced to the melt, the mole fraction of CO_3^{2-} was lower than that of Li_2O. Therefore, we can neglect any gas dissolution not leading to the formation of carbonate ions and hypercarbonates such as

$Li_2(CO_3)_n$ ($n > 1$). The CO_2 solubility (X_{CO2}) was evaluated by using equations (11) and (12):

$$X_{CO2} = N_{CO2}/(N_{Li2O} + N_{LiCl}) \quad (11)$$

$$N_{CO2} = \Delta w/M_{CO2} \quad (12)$$

In the above equation, N_{Li2O} and N_{LiCl} are the initial molar quantities of Li_2O and LiCl added to the crucible, respectively, and Δw (g) is the mass difference caused by the dissolution of CO_2 gas. N_{CO2} is the molar quantity of dissolved CO_2, and M_{CO2} (g/mol) is the molecular weight of CO_2.

To measure the maximum solubility of CO_2, CO_2 should be saturated in the molten salt. Therefore, Fig. 3 shows the relationship between the exposure time and CO_2 concentration to allow an estimation of the CO_2 saturation time. When X_{Li2O} is 0.2, X_{CO2} should also be 0.2 at a holding time of 14.4 ks. However, X_{CO2} slightly decreased when the holding time was increased to 172.8 ks. Because a small amount of LiCl was deposited on the colder part of the reaction vessel, mass loss due to vaporization of the molten salt could not be neglected. When X_{Li2O} was 0.6, X_{CO2} increased from a holding time of 14.4 ks to a holding time of 32.4 ks, but decreased when the holding time

1 further increased 172.8 ks because of the considerable mass loss. Therefore, 86.4 ks was
2 chosen for further analysis as a dissolution time at which CO_2 gas was saturated but the
3 effect of the vaporization was insignificant as compared to that observed at a holding
4 time of 172.8 ks. The mass loss due to the evaporation of the molten salt was corrected
5 for as described in the next section.
6
7 *3.3. Effect of salt evaporation*
8 Because the sample in the crucible constantly loses mass when the molten salt is kept
9 at a high temperature, it is necessary to evaluate the mass loss due to the molten salt
10 vaporization at 923 K. The mass loss was experimentally measured by keeping the
11 samples at 923 K under an Ar atmosphere.
12 Fig. 4 shows the amount of salt that evaporates within 86.4 ks as a function of the
13 Li_2O concentration. The amount of evaporation was independent of the Li_2O
14 concentration over a wide range, as long as the crucible was the same size. The
15 correction value $\Delta w_{cor.}$ (g) was determined by taking the average of the amounts of
16 evaporated salt for the different experiments. The following compensating equation
17 (13) was deduced from equation (12):
18

$$N_{CO2}^{*} = (\Delta w - \Delta w_{cor.})/M_{CO2} \quad (13)$$

The compensated solubility of the CO_2 gas in the molten salt, $X_{CO2,\ meas.}$ was thus calculated by considering the amount of salt that evaporated. However, this compensation hardly affected the CO_2 solubility: its contribution was less than 1%.

3.4. Solubility of CO_2 gas in molten LiCl

Table 2 shows the CO_2 solubility data. $X_{Li2O,id.}$ is the target composition before weighing, and $X_{Li2O,meas.}$ is the measured composition calculated from the amounts of LiCl and Li_2O. X_{CO2} is the molar fraction of dissolved CO_2 calculated by neglecting the error of the electric balance and the amounts of evaporated salt. $X_{CO2,high}$ and $X_{CO2,low}$ are the maximum and minimum values when the error of electric balance and the amounts of evaporated salt were taken into consideration. $X_{CO2,ave}$ is the average of $X_{CO2,high}$ and $X_{CO2,low}$. The difference between $X_{CO2,high}$ and $X_{CO2,low}$ was very small, less than 1%.

Fig. 5 shows the relationship between the compensated CO_2 solubility and the measured concentration of Li_2O at 923 K for an exposure duration of 86.4 ks. Three partial pressures of CO_2 (P_{CO2}) were selected: 1.0, 0.5, and 0.1 atm. The CO_2 solubility

increases linearly with increasing initial Li_2O concentration at P_{CO2} = 1.0 and 0.5 atm. The broken line in Fig. 5 represents the ideal CO_2 solubility when all the O^{2-} in the molten salt reacts with the CO_2 gas. As discussed in section 3.2, the CO_2 gas was saturated for a wide range of Li_2O concentrations. When P_{CO2} was 1.0 and 0.5 atm, the CO_2 solubility also approached the ideal solubility for a wide range of Li_2O concentrations, as shown in Fig. 5. There is a strong positive correlation between the CO_2 solubility and Li_2O concentration, with a correlation coefficient of 0.9998. Regression analysis revealed that the slope of the straight line showing the proportional relationship between the two variables was 95% of the slope for the ideal relationship. Thus, 95% of the initial amount of O^{2-} in the molten salt well reacted with CO_2 gas to form CO_3^{2-}.

However, when P_{CO2} was 0.1 atm, the solubility of CO_2 was clearly different from the other partial pressures of CO_2. The equilibrium constant of reaction (8) thermodynamically depends only on the temperature, not on P_{CO2}. Therefore, the decrease in CO_2 solubility corresponds to a change in the ratio between the thermochemical activities of CO_3^{2-} and O^{2-} with decreasing P_{CO2}.

The reason why the CO_2 solubility was constant over a wide range of Li_2O at P_{CO2} = 0.1 atm is explained below. According to Usami et al., the solubility of Li_2O in the

LiCl melt is only about 12 mol% at 923 K [17]. Thus, the residual Li_2O exists as a solid when more than 12 mol% Li_2O is present. In this study, the concentration of Li_2O initially ranged between 0 and 60 mol%, and some portion of Li_2O existed as a solid prior to the injection of the gas and in the initial stages of CO_2 dissolution. Li_2O could turn into Li_2CO_3 and then form a LiCl-Li_2CO_3 molten salt. However, when P_{CO2} is as low as 0.1 atm, the CO_2 gas may not be well saturated in the molten salt, and a small amount of undissolved Li_2O may remain unreacted. This problem is challenging to solve, because, for example, extending the CO_2 dissolution time causes an increase in mass loss due to vaporization of the molten salt.

4. Discussion

When the Li_2O content is 60 mol% at P_{CO2} = 1.0 and 0.5 atm, more than 95% of the reacted Li_2O can be expected to exist as CO_3^{2-}, as shown in Fig. 5. Similar works on the dissolution of CO_2 gas in a mixture of a chloride and an oxide were reported by Maeda and Ikeda [22] and by Hashizume et al. [10]. They found that the CO_2 solubility in the $CaCl_2$-CaO melt followed a linear relationship with the initial amount of CaO. A similar linear relationship was also found in the present study on the LiCl-Li_2O system, as shown in Fig. 5. Whereas thermogravimetry was used to measure the mass

difference in previous work [7], the work presented here proves that similar results can be obtained by using a simple apparatus. The data accumulation method developed in this study can also be applied at the other temperatures and pressures to study oxide reduction using molten salt electrolysis in expanded temperature or pressure ranges. For example, Ijije et al [26] recently reported the CO_2 decomposition using the molten salts containing Li_2CO_3. Their operating temperature is in the range of 723K and 1173 K by mixing with Na_2CO_3 and K_2CO_3. The CO_2 dissolution data for the wider temperature range and at the various mixtures are required for the further precise operation of CO_2 decomposition.

It is noted that the maximum solubility of CO_2 in the LiCl-Li_2O melt is significantly higher than the values reported in previous studies for the $CaCl_2$-CaO melt. This indicates a strong affinity between Li_2O and CO_2 gas at 923 K. The solubility of CO_2 in the $CaCl_2$-CaO melt was also studied at temperatures higher than 923 K, at which the thermal stability of $CaCO_3$ is weaker. The solubility at P_{CO2}=1 atm is useful for evaluating the concentration of CO_2 close to the anode in the OS and FFC processes, because O^{2-} at the carbon anode reacts with carbon to form CO_2 gas bubbles at P_{CO2}=1.

When the metallic oxide is reduced at the cathode in carbonate ion-rich molten salt in

the OS method, carbon contamination of the reduction product may be driven by reactions (8) and (14) [15, 26]:

$$CO_3^{2-} + 4e^- = C + 3O^{2-} \quad (14)$$

Therefore, the cathodic potential in this process must be kept at the voltage that carbonate ions cannot decompose to contaminate the product as carbon or a carbide. In contrast, the data obtained at $P_{CO2} < 1$ atm are informative about the CO_2 decomposition process at low temperatures such as 923 K. When the gaseous CO_2 is decomposed in the OS method, a mixture of CO_2 and Ar gas is introduced at the cathode that forms carbon, and the partial pressure of CO_2 in the gas bubbles is lower than 1 atm [14]. When LiCl-Li_2O molten salt is used to decompose gaseous CO_2, the CO_2 gas bubbling changes the composition of the residual molten salt from LiCl-Li_2O to LiCl-Li_2O-Li_2CO_3. In this context, the CO_2 solubility obtained in this work will be valuable for future applications.

Supposing that the decrease in CO_2 solubility at P_{CO2} = 0.1 atm is due to the precipitation of Li_2O(s), the phase equilibria in the LiCl-Li_2O-Li_2CO_3 ternary system were predicted, as shown in Fig. 6. The maximum solubilities of Li_2CO_3 and Li_2O in liquid LiCl correspond to the compositional points A and B in Fig. 6, respectively. Assuming that the maximum solubility of CO_2 in liquid LiCl at P_{CO2} = 0.1 atm is given

by point C, three-phase equilibrium among the LiCl-rich liquid, solid Li_2O, and solid Li_2CO_3 is predicted as the shaded triangle in Fig. 6. The solidus line is shown as a broken line. From the experimental results, at P_{CO2} > 0.5 atm, the two-phase equilibrium between the LiCl melt and Li_2CO_3 is achieved. When P_{CO2} < 0.1 atm, the LiCl melt should form an equilibrium with Li_2O(s). Therefore, the three-phase equilibrium can exist when P_{CO2} is between 0.1 and 0.5 atm. Since the pressure required to decompose Li_2CO_3 to CO_2 gas and Li_2O is evaluated as 2.2×10^{-5} atm from the thermodynamic data [23], the P_{CO2} for the three-phase equilibrium is higher than 2.2×10^{-5} atm. Therefore, the isobars of oxygen between 2.2×10^{-5} and 0.1 atm in the LiCl-rich liquid connect with the solid solution of Li_2O and enter into the single-phase region of Li_2O. These isobars also finally enter the region of the Li_2CO_3 solid solution. A phase equilibrium between Li_2CO_3 and Li_2O should exist over a wide range of Li_2CO_3 and Li_2O contents, as shown by regions I and II in Fig. 6. Such an Li_2CO_3(s)-Li_2O(s) equilibrium cannot exist if Li_2CO_3 and Li_2O are insoluble. The existence of this equilibrium over a wide range of Li_2CO_3 and Li_2O contents may cause the inversion in the relationship between CO_2 solubility and P_{CO2} close to the Li_2CO_3-Li_2O quasi-binary system.

5. Conclusions

The solubility of CO_2 gas in LiCl-Li_2O was determined experimentally by measuring the mass change due to CO_2 gas dissolution. A small amount of molten salt was evaporated when the melt was held at 923 K, which influenced the mass change measured for the compositional range considered here. This mass change was subtracted from the measured mass change, and the measured data were well compensated, although this correction to the CO_2 solubility was less than 0.1%. After this correction, it was found that a molar quantity of CO_2 gas as large as 95% of the molar quantity of Li_2O could dissolve into the molten salts in the compositional range 0–60 mol% Li_2O. The formation of Li_2CO_3 due to CO_2 dissolution and its dissolution into the LiCl melt were observed by XRD analysis. The dissolution behavior of CO_2 gas is identical at P_{CO2} = 1.0 and 0.5 atm. However, the possible precipitation of Li_2O at P_{CO2} = 0.1 atm was discussed on the basis of the ternary phase equilibrium.

List of symbols

T	Experimental temperature [K]
t	Dissolution time of CO_2 gas
X_i	Mole fraction of chemical species "i"

X_{CO2}	Mole fraction of dissolved CO_2
N_i	Molar quantities of chemical species "*i*"
M_i	Molecular weight of chemical species "*i*"
Δw	Amount of evaporated salt
P_{CO2}	Partial pressure of CO_2

Subscripts

cor.	corrected
ave.	averaged
id.	ideal
meas.	Measured

6. Acknowledgements

The authors thank Ms Mika Kitamura of Hokkaido University for her experimental assistance. They also appreciate financial support from the Japan Science and Technology Agency (JST) – Advanced Low Carbon Technology Research and Development Program (ALCA).

References

[1] K. Hirota, T.H. Okabe, F. Saito, Y. Waseda, K.T. Jacob, J. Alloy. Compd. 282 (1999) 101-108.

[2] R.O. Suzuki, M. Aizawa, K. Ono, J. Alloy. Compd. 288 (1999) 173–182.

[3] R.O. Suzuki, S. Inoue, Metall. Mater. Trans. B, 34B (6) (2003) 277-286.

[4] G.Z. Chen, D.J. Fray, T.W. Farthing, Nature, 407 (2000) 361-364.

[5] K. Yasuda, T. Nohira, K. Amezawa, Y.H. Ogata, Y. Ito, J. Electrochem. Soc. 152 (2005) D69-D74.

[6] S. Lee, J. Hur, C. Seo, J. Ind. Eng. Chem. 14 (2008) 651-654.

[7] S.Jeong, J.Jung, C.Seo, S.Park, J.Alloys.Compounds, 440 (2007) 210-215.

[8] W. Park, J. Hur, S. Hong, E. Choi, H. Im, S. Oh, J. Lee, J. Nucl. Mater., 441 (2013) 232-239.

[9] Y.Oka, R.O.Suzuki, J. Jpn. Inst. Met., 72(2008)181-187.

[10] J. Hashizume, Y. Oka, R.O. Suzuki, Proceedings of 2008 Joint Symposium on Molten Salts, (2008) 128-133.

[11] C.Wagner, Metall. Trans. B, 6 (1975) 405-409.

[12] T.Kawahara, S.Shibata, N.Sano, Proc. 5th Int. Iron and Steel Congress, Washington, D.C. (1986) 488.

[13] T. Ikeda, M. Maeda, Tetsu to Hagané, 5 (75) (1989) 742-749.

[14] K. Otake, H. Kinoshita, R.O. Suzuki, Electrochim. Acta, 100 (2013) 293-299.

[15] B. Kaplan, H. Groult, A. Barhoun, F. Lantelme, T. Nakajima, V. Gupta, S. Komaba, N. Kumagai, J. Electrochem. Soc. 149 (5) (2002) D72-D78.

[16] J. M. Sanster, A. D. Pelton, Special Report to the Phase Equibria Program, American Ceramic Society; Westerville, Ohio, (1987) 22-24.

[17] T. Usami, M. Kurata, T. Inoue, H.E. Sims, S.A. Beetham, J.A. Jenkins, J. Nucl. Mater. 300 (2002) 15-26.

[18] H. Flood, T. Forland, K. Motzfeldt, Acta Chim. Scand. 6 (1952), 257-269.

[19] G.J. Janz, F. Saegusa, Electrochim. Acta, 7 (1962), 393-398.

[20] A.T. Ward, G.J. Janz, Electrochim. Acta, 10 (1965), 849-857.

[21] M.D. Ingram, G.J. Janz, Electrochim. Acta, 10 (1965), 783-792.

[22] M. Maeda, A. Mclean, ISS transactions, 8 (1987) 23-27.

[23] A. Roine, HSC Chemistry, ver.6.12, Outotec Res. Oy. Pori, Finland, 2007.

[24] D. C. Montgomery, Design and Analysis of Experiments, 7th ed., Wiley, New York, 2008.

[25] J. Hur, S. Jeong, H. Lee, Nucl. Eng. Technol., 42 (2010) 73-78.

[26] H.V. Ijije, T.C. Lawrence. G.Z. RSC Adv., 4 (2014) 35808-35807.

Table caption

Table 1 Chemicals description.

Table 2 Experimental results for each condition.[a]

Figure captions

Fig. 1 Experimental set-up used in the present study.

Fig. 2 (a) XRD pattern of the sample not subjected to CO_2 dissolution.

(b) XRD pattern of the sample after dissolution of CO_2.

Fig. 3 Time-dependent change of the mass difference of the crucible.

Fig. 4 Amount of the evaporated salt evaluated by mass loss during heating in Ar gas at 923 K for 86.4 ks.

Fig. 5 Amount of dissolved CO_2 at three conditions.

Fig. 6 Phase equilibria in the LiCl-Li_2O-Li_2CO_3 ternary system.

Component	Source	Mass fraction purity	Purification method
Lithium Oxide	Strem Chemicals Co.	>99%	None
Lithium Chloride	Wako Chemical Co.	>99.5%	None
CO_2	Hokkaido Air Water Co.	>99.5%	None
Ar	Hokkaido Air Water Co.	>99.999%	None

No.	$X_{Li2O,\ id.}$	$X_{Li2O,\ meas.}$	X_{CO2}	$X_{CO2,high}$	$X_{CO2,low}$	$X_{CO2,ave.}$	P_{CO2}	t
1	0.200	0.200	0.1862	-	-	-	1.000	14.4
2	0.600	0.600	0.3891	-	-	-	1.000	14.4
3	0.200	0.201	0.1903	-	-	-	1.000	32.4
4	0.200	0.201	0.1778	-	-	-	1.000	32.4
5	0.600	0.602	0.5540	-	-	-	1.000	32.4
6	0.600	0.602	0.5740	-	-	-	1.000	32.4
7	0.050	0.050	0.033	0.035	0.034	0.0345	1.000	86.4
8	0.100	0.100	0.087	0.089	0.088	0.0885	1.000	86.4
9	0.150	0.150	0.137	0.139	0.138	0.1385	1.000	86.4
10	0.200	0.201	0.183	0.185	0.184	0.1845	1.000	86.4
11	0.300	0.302	0.279	0.281	0.281	0.281	1.000	86.4
12	0.400	0.402	0.377	0.379	0.379	0.379	1.000	86.4
13	0.600	0.602	0.570	0.573	0.573	0.573	1.000	86.4
14	0.150	0.151	0.131	0.133	0.132	0.1325	0.500	86.4
15	0.300	0.301	0.283	0.285	0.284	0.2845	0.500	86.4
16	0.450	0.451	0.430	0.433	0.432	0.4325	0.500	86.4
17	0.600	0.601	0.573	0.576	0.575	0.5755	0.500	86.4
18	0.150	0.150	0.096	0.098	0.096	0.097	0.100	86.4
19	0.300	0.301	0.129	0.131	0.130	0.1305	0.100	86.4
20	0.450	0.451	0.133	0.135	0.134	0.1345	0.100	86.4
21	0.150	0.150	0.111	0.113	0.112	0.1125	0.100	86.4
22	0.300	0.300	0.124	0.126	0.124	0.125	0.100	86.4
23	0.450	0.452	0.140	0.142	0.141	0.1415	0.100	86.4
24	0.200	0.200	0.155	-	-	-	1.000	172.8
25	0.600	0.600	0.572	-	-	-	1.000	172.8

- Not measured

a An uncertainties are $U(P_{CO2}) = \pm 0.004$ atm , $U(T) = \pm 1$ K.

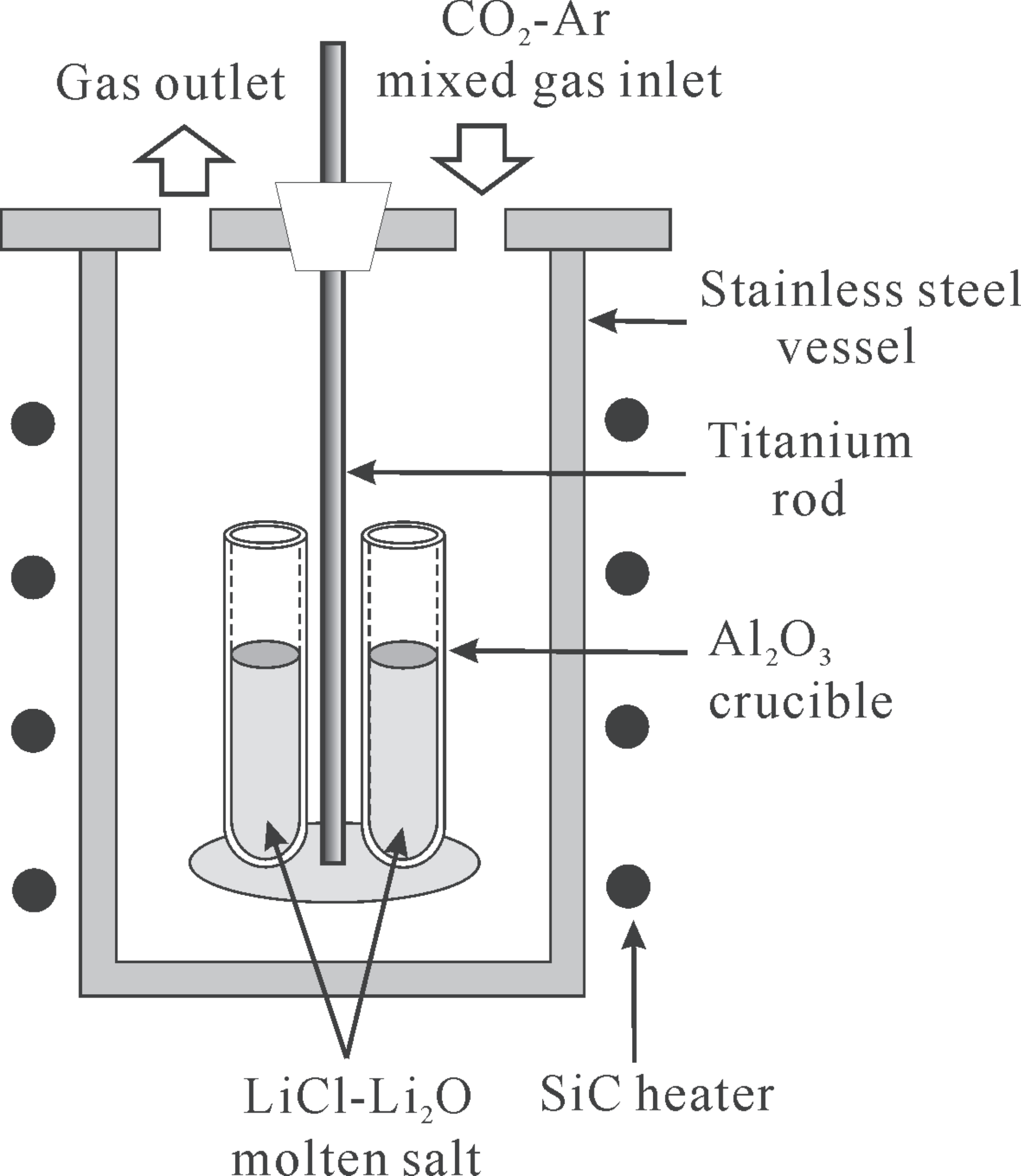
CO_2-Ar
mixed gas inlet
Gas outlet
Stainless steel
vessel
Titanium
rod
Al_2O_3
crucible
$LiCl$-Li_2O
molten salt
SiC heater

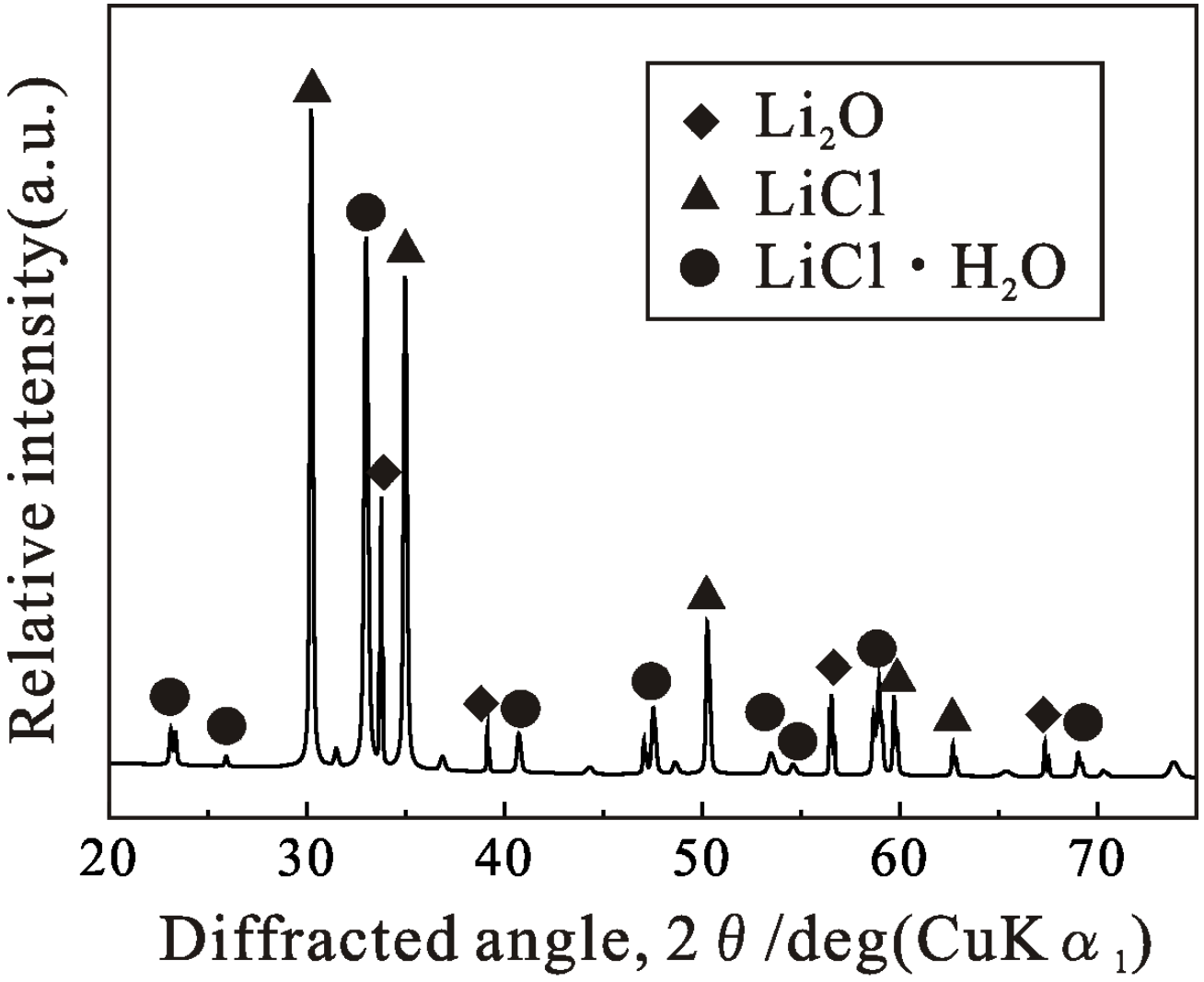
Li2O
LiCl
LiCl · H2O
Relative intensity(a.u.)
20
30
40
50
60
70
Diffracted angle, 2 θ /deg(CuK α 1)

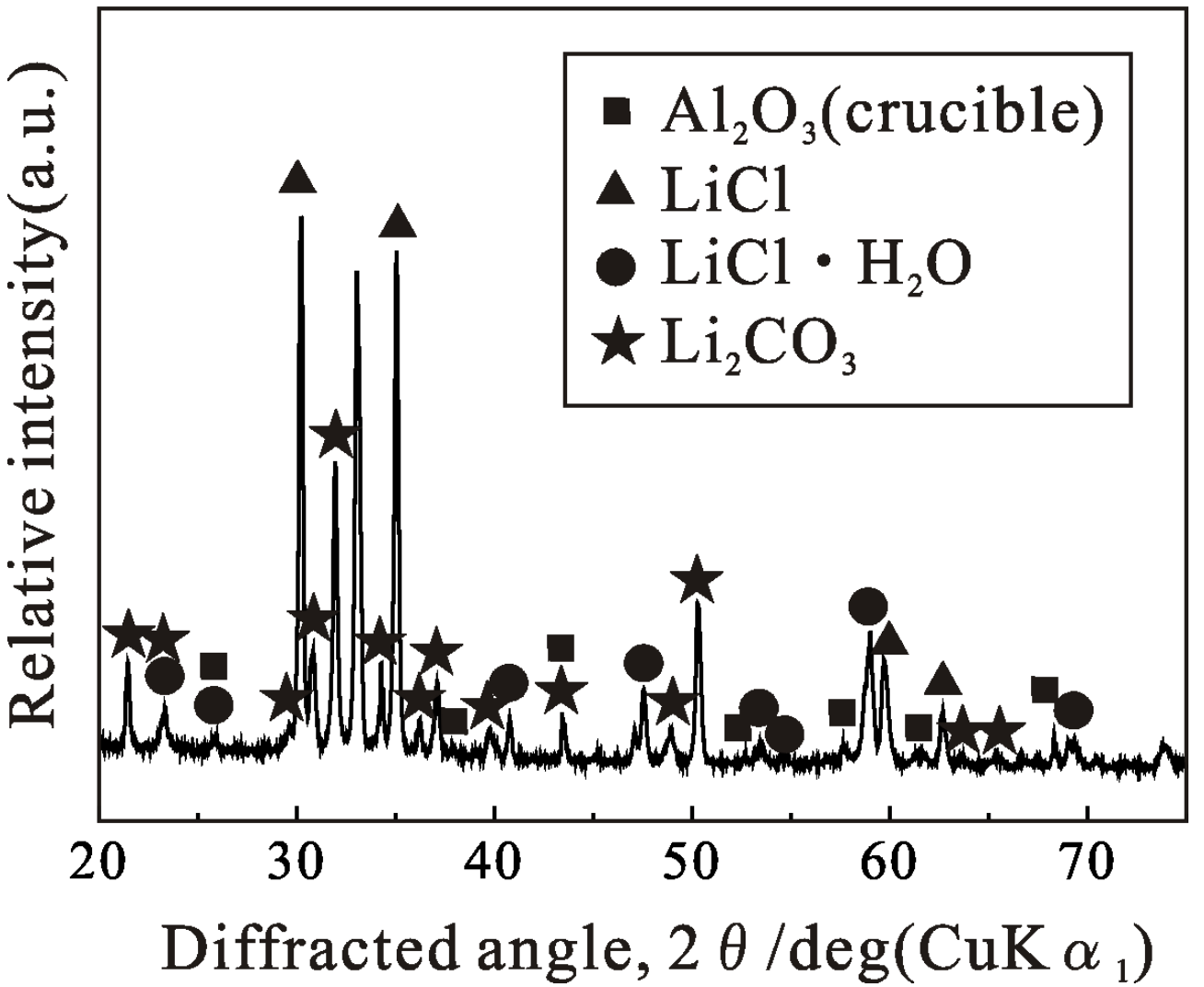
Al2O3(crucible)
LiCl
LiCl · H2O
Li2CO3
Relative intensity(a.u.)
20
30
40
50
60
70
Diffracted angle, 2 θ /deg(CuK α 1)

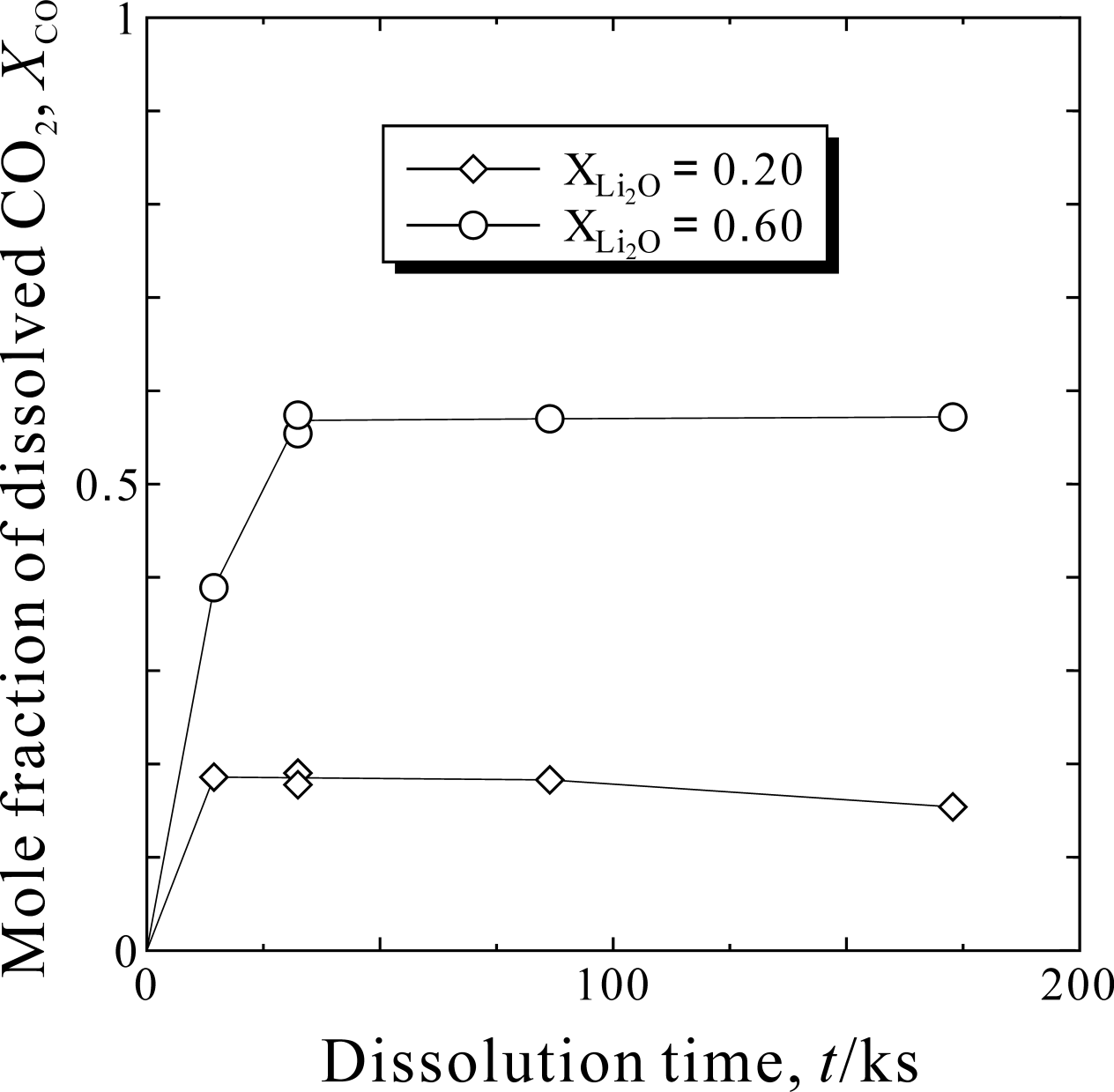
Mole fraction of dissolved CO_2, X_{CO_2}
1
0.5
0
0
100
200
Dissolution time, t/ks
X_{Li_2O} = 0.20
X_{Li_2O} = 0.60

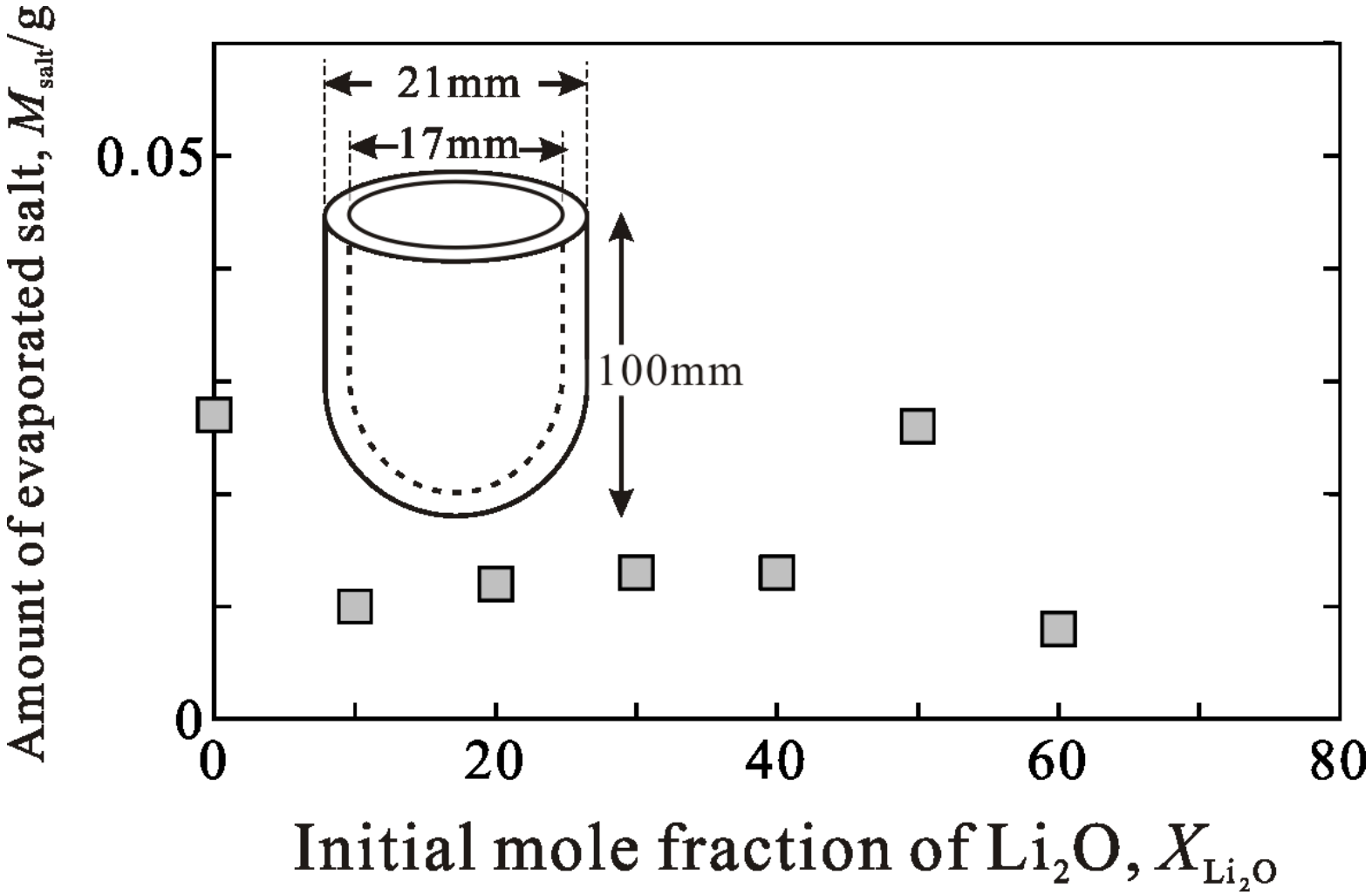
Amount of evaporated salt, M_{salt}/g
0.05
0
21mm
17mm
100mm
0
20
40
60
80
Initial mole fraction of Li_2O, X_{Li_2O}

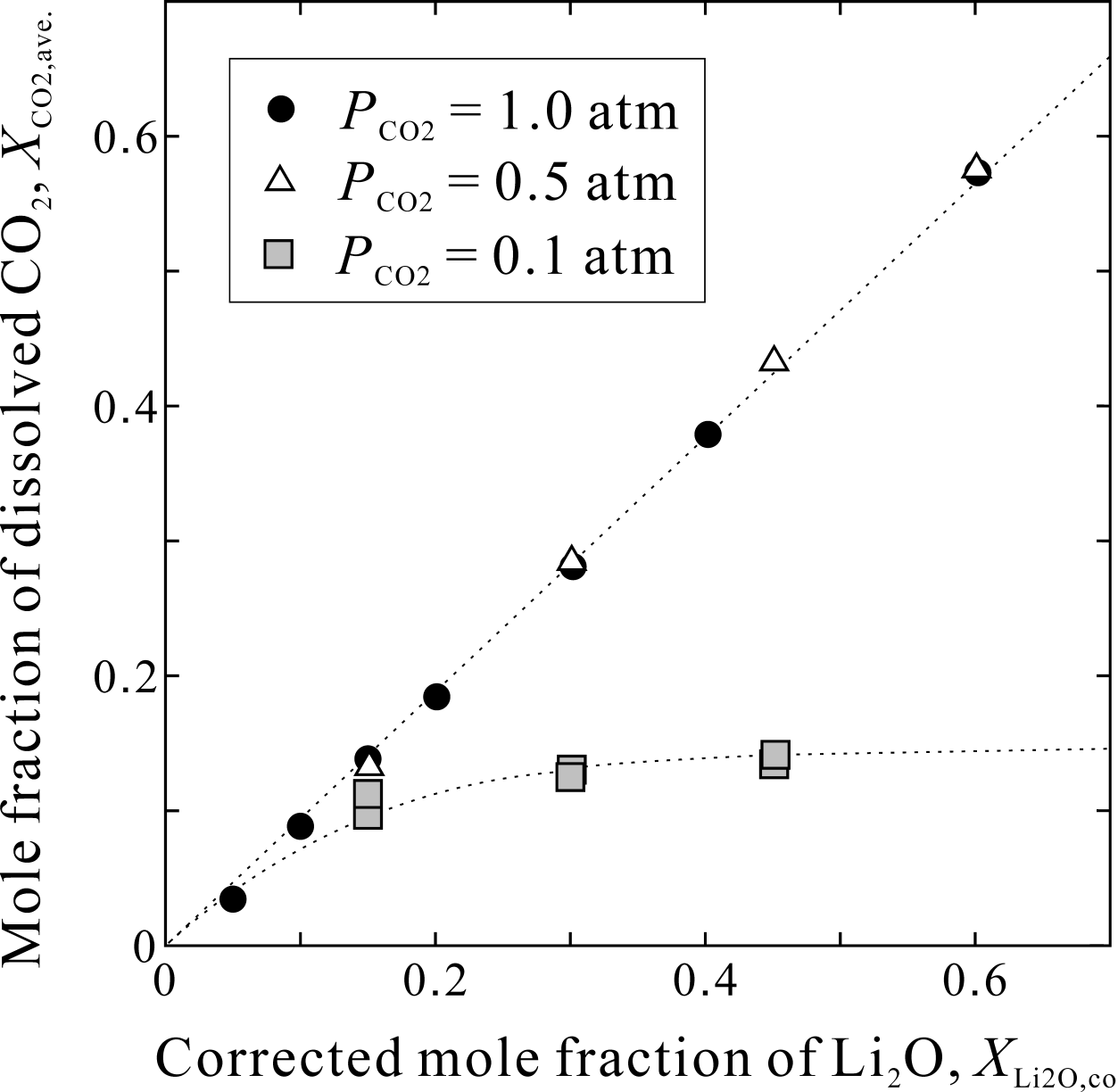
$P_{CO2} = 1.0$ atm
$P_{CO2} = 0.5$ atm
$P_{CO2} = 0.1$ atm
Mole fraction of dissolved CO_2, $X_{CO2,ave.}$
Corrected mole fraction of Li_2O, $X_{Li2O,cor.}$
0
0.2
0.4
0.6

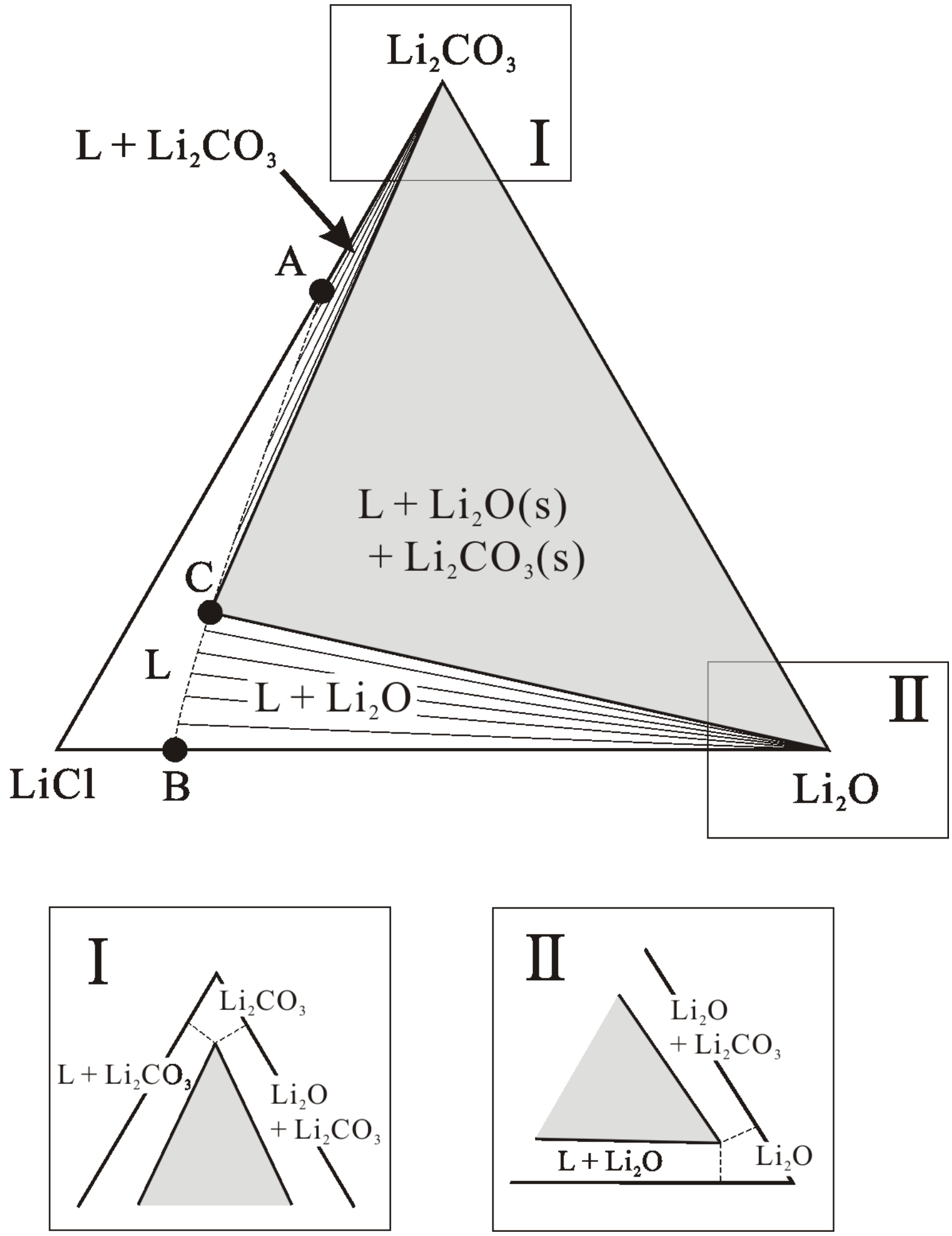
Li2CO3
I
L + Li2CO3
A
L + Li2O(s)
+ Li2CO3(s)
C
L
L + Li2O
II
LiCl
B
Li2O
I
Li2CO3
L + Li2CO3
Li2O
+ Li2CO3
II
Li2O
+ Li2CO3
L + Li2O
Li2O